Jet Deflection by Very Weak Guide Fields during Magnetic Reconnection

M. V. Goldman, G. Lapenta, D. L. Newman, S. Markidis, and H. Che

Phys. Rev. Lett. **107**, 135001 — Published 19 September 2011
DOI: 10.1103/PhysRevLett.107.135001

Jet deflection by very weak guide fields during magnetic reconnection

M. Goldman,[1] G. Lapenta,[2] D. Newman,[1] S. Markidis[2] and H. Che[1]

[1] *Dept. of Physics and CIPS, University of Colorado, Boulder, CO 80309, USA*

[2] *Centrum voor Plasma-Astrofysica, Katholieke Universiteit Leuven, Belgium*

(Submitted to PRL July 16, 2010)

Abstract

Previous 2-D simulations of reconnection using a "standard" model of initially antiparallel magnetic fields have detected electron jets outflowing from the x-point into the ion outflow exhausts. Associated with these jets are extended "outer electron diffusion regions." New PIC simulations with ion/electron mass ratios as large as 1836 (an H^+ plasma) now show that the jets are strongly deflected and the outer electron diffusion region is broken up by a very weak out-of-plane magnetic guide field, even though the diffusion rate itself is unchanged. Jet outflow and deflection are interpreted in terms of electron dynamics and are compared to recent measurements of jets in the presence of a small guide field in Earth's magnetosheath.

PACS numbers: 52.35.Vd, 94.30.cp, 52.65.Rr, 52.20.Dq

Introduction

Magnetic reconnection is currently one of the most actively studied processes in plasma physics. It is believed to be responsible for solar flares, coronal mass ejections and magnetospheric substorms. The study of *electron-scale* processes associated with magnetic reconnection in the magnetosphere is one of NASA's highest priorities — to culminate in 2014 with the launch of the Multiscale Magnetosphere Satellites that will be able to resolve electron features of reconnection up to 100 times faster than existing satellites.

Many Particle-In-Cell (PIC) simulation[i,ii,iii] studies of electron-scale physics during reconnection employ a common ("standard") model of 2-D *antiparallel* reconnection in which the initial magnetic field, $\mathbf{B} = \hat{x}\, B_0 \tanh(y/\Delta y)$, lies entirely in a plane (here taken as the x-y plane), as in early MHD simulations. There are many predictions from such standard PIC simulations which are often taken as essential signatures of reconnection — symmetric Hall currents and fields, symmetric particle densities, and particle outflow centered in the exhausts. Such outflow includes electron jets, coherently directed and extended deep into the exhausts ("x"-direction), accompanied by elongated "outer diffusion regions."

However, just as with 2D MHD simulations[iv], it is now becoming evident that these features are dramatically changed by even small departures from the assumptions of the "standard" model. In particular, the addition of a guide field, $B_g \hat{z}$ much smaller than the asymptotic reconnecting field component, B_0 can have profound effects.[v]

In this Letter, we provide evidence from PIC reconnection simulations[vi] (with an ion to electron mass ratio of up to M/m = 1836) that guide fields of $B_g = 0.05B_0$ and $0.1B_0$

are sufficient to deflect and distort the jets from the x-axis towards separatrix legs, while the reconnection rate remains essentially unchanged. Cluster measurements[vii] reported in PRL during symmetric magneto-sheath reconnection have been interpreted as evidence for an elongated narrow jet in v_{ex} of width $9d_e = 9c/\omega_{pe}$ = 11km (Fig. 1). Asymptotic reversing B_x fields of $B_0 = \pm 40$ nT were measured both at the exhaust entry and exit. A guide field of B_g = 7 nT was measured at the exhaust entry *and* at the inferred jet location itself (Fig. 1a). Hence, $B_g = 0.16B_0$ to good accuracy. Such jets would be consistent with outer diffusion regions similar to those found in explicit PIC simulations[i,ii] with *no* guide field and ion-to-electron mass ratios, M/m = 25. The new reconnection simulations in this Letter *do show* jet deflection using M/m as high as 1836 and guide fields, B_g, *smaller than the measured* $B_g = 0.16B_0$. This disagreement will be addressed in the conclusion.

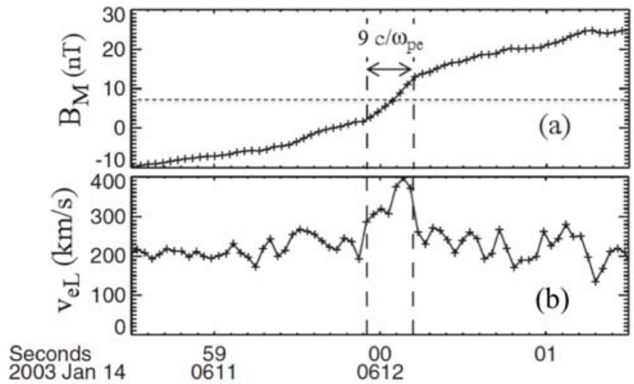

Figure 1: (a): Measured $B_M = B_z$ with B_g = 7 nT (dashed horizontal line). (b) Inferred jet in $v_{eL} = v_{ex}$. (Frm Ref vii).

New reconnection simulations with very small guide fields

In order to determine how electron jets depend on the guide field, new implicit[vi] 2D PIC simulations of spontaneous reconnection have been performed. The initial state is a perturbed Harris equilibrium, with $B_x(y) = B_0 \cdot \tanh(y/\Delta y)$, where Δy is the initial current sheet thickness, taken here to be $d_i/2$. Initial electron and ion temperatures are $T_{e0}/m_e c^2 = (v_{the0}/c)^2 = 2 \times 10^{-3}$, and $T_{i0} = 5T_{e0}$. The background density is n_b =

$0.1n_0$, where n_0 is the peak initial density.

In Fig 2a, $v_{ex}(x,y)/v_{the0}$, the dominant component of the electron flow velocity, $\mathbf{v_e}/v_{the0}$, is compared at the same time, $\Omega_i t = 14.2$, in three reconnection simulations, for M/m = 1836 and various $\mathbf{B}_g$. Note the expanded aspect ratio of y to x.

For B_g =0 (Fig. 2a), incipient outgoing collimated jets flow out from the x-point along

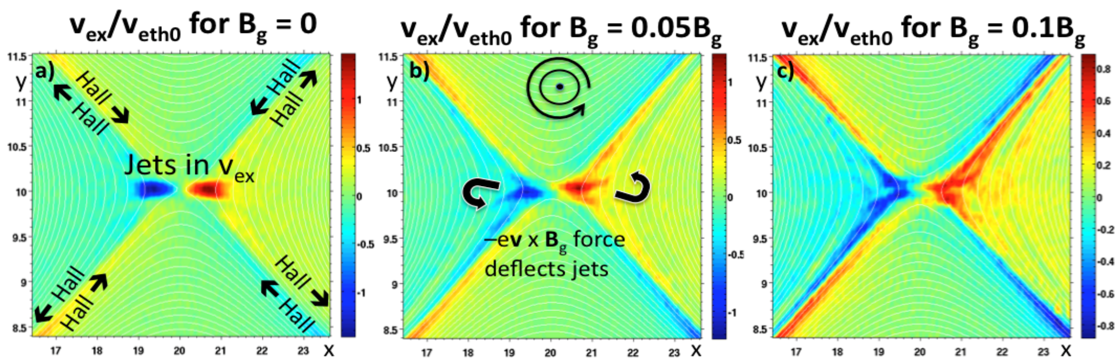

Figure 2: Deflection of jet in x-velocity of electrons, v_{ex}/v_{eth0}, by small guide fields (M/m = 1836). a) $B_g = 0$; b) $B_g/B_0 = 0.05$; c) $B_g/B_0 = 0.1$. x and y in units of d_i. Note expanded aspect ratio.

the ±x-axis at y = $10d_i$. However, even for $B_g = 0.05B_0$, (Fig. 2b), the jets are split and deflected. For $B_g = 0.1B_0$ (Fig. 2c) the deflection of jets by the Lorentz force associated with B_g has resulted in dominant beams elongated along appropriate separatrix legs.

The net electric plus magnetic force[i,ii,viii,ix] accelerating $\mathbf{v}_e(x,y)$ is, $\mathbf{F}(x,y) = -e\boldsymbol{\mathcal{E}}(x,y)$, where $\mathcal{E}$ is defined as a generalized "field," $\boldsymbol{\mathcal{E}} = \mathbf{E} + \mathbf{v} \times \mathbf{B}/c$. In Fig. 3, components of $\boldsymbol{\mathcal{E}}(x,y)$ are plotted at the same time, $t\Omega_i = 14.2$ as in Fig. 2. For B_g= 0 (Fig. 3a), the in-flowing electron y-velocity, $v_{ey}(x,y)$ is essentially frozen-in (= $\pm cE_z/B_x$) just above and below the central (blue) "inner" diffusion region. The flanking (red) regions are the early "outer" diffusion regions[i,ii.]

For the case $B_g = 0.1B_0$, (Fig. 3b) the inner diffusion region is distorted, but more significantly, the outer diffusion region is no longer elongated in x or collimated in y. The reconnection rate, however, is not significantly changed.

Figs. 3c and 3d show $\mathcal{E}_x$ and $\mathcal{E}_y$, respectively, for $B_g = 0$. The yellow rectangles enclose regions where, to a good approximation, $\mathcal{E}_x \propto -x$ and $\mathcal{E}_y \propto y$. The y-boundaries of this region are the y-boundaries of the jets (Fig. 1a) (same as y-boundaries of the *current sheet)*. The boundaries at x = $\pm 0.4d_i$ are at about half the values of the x-boundaries of the jets. The force, $-e\mathcal{E}_x \propto x$, accelerates electrons *away from the x-point* at x = $20d_i$ to form the outgoing jets. The dominant contribution to $-e\mathcal{E}_x$ in this region is the Lorentz force, $ev_{ez}B_y(x)/c$, due to the out-of-plane almost-uniform velocity v_{ez} of the electron *current sheet* and the in-plane $B_y(x)$ of the *reconnected* field lines.[i,ii] E_x is

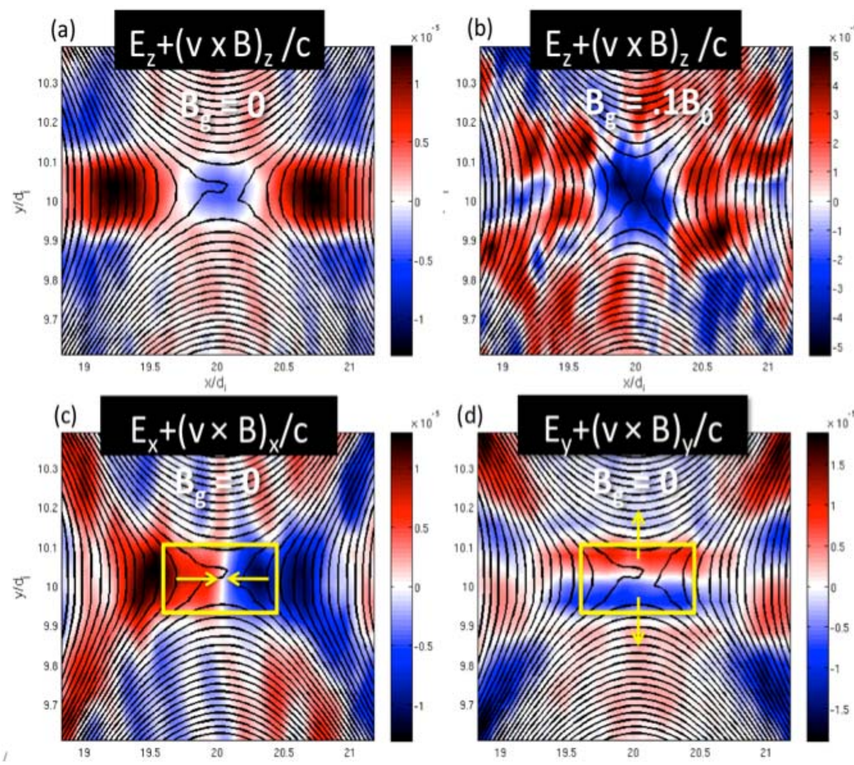

Figure 3: Components of electric-magnetic force "field," $\mathcal{E}$(x, y) = **F/(-e)** = **E**+(**v** x **B**)/c in simulation units, $\sqrt{4\pi n_0 m_i c^2}$ (M/m = 1836, $t\Omega_i$ = 14.2). a) $\mathcal{E}_z$ for B_g = 0; b) Same for $B_g = 0.1B_0$, c) $\mathcal{E}_x$ and d) $\mathcal{E}_y$, for B_g =0. Yellow arrows show direction of $\mathcal{E}_x$ and $\mathcal{E}_y$. Rectangles enclose "linear" regions.

about half as large as $v_{ez}B_y(x)/c$ inside this region but dominates outside where it can cause oscillations (trapping) in x in both the in-flow region and the exhaust.[ii,ix]

In Fig. 3d, $-e\mathcal{E}_y(y) \propto -y$ is a *restoring* force in y inside the yellow box. It *traps the jet in the y-direction* and keeps it from expanding in y. Once again, the Lorentz force, $ev_{ez}B_x(y)/c$ contribution is about twice as big as the *(Hall) electric field* force, $-eE_y$.

Electron dynamics in linear region

The dynamical equations for the 2D motion of an electron due to in-plane fields $E_{x,y}(x,y)$ and $B_{x,y}(x,y)$ underlying Fig. 3c and 3d, together with the Lorentz force of a weak guide field, $B_g \leq 0.1B_0$ are:

$$\text{(1a)}\quad \ddot{x} + \frac{e}{m}\left[E_x(x,y) - \frac{\dot{z}B_y(x,y)}{c}\right] = -\Omega_{eg}\dot{y}$$

$$\text{(1b)}\quad \ddot{y} + \frac{e}{m}\left[E_x(x,y) + \frac{\dot{z}B_x(x,y)}{c}\right] = \Omega_{eg}\dot{x}$$

Here, $\Omega_{eg} = eB_g/m_ec$. Assume now that $\dot{z}$ is equal to its initial value, $\dot{z}_0$, which, in turn, is set equal to v_{ez} of the current sheet in the linear region, where it is essentially independent of x and y. Neglect of the dynamical evolution of $\dot{z}$ away from its initial value, $\dot{z}_0$ has been verified numerically and sets this treatment apart from that of the so-called Speiser orbits.[x] For $B_g = 0$ the square brackets in eqns. (1) can be approximated as $\mathcal{E}_x(x) \propto -x$ and $\mathcal{E}_y(y) \propto y$ in the yellow boxes in Fig. 3c,d. They remain approximately stationary and equal to their values at time 14.2 throughout the electron motion. The eqns. of motion in the linear region are:

$$\text{(2)}\quad \ddot{x} - \gamma_x^2 x \approx -\Omega_{eg}\dot{y}, \quad \ddot{y} + \omega_y^2 y \approx \Omega_{eg}\dot{x}$$

The linear coefficients are $\gamma_x^2 \equiv -\omega_e^2\left[\partial_{x'}\mathcal{E}_x^{sim}(x')\right]_{x'=0} > 0$ and $\omega_y^2 \equiv \omega_e^2\left[\partial_{y'}\mathcal{E}_y^{sim}(y')\right]_{y'=0} > 0$.

The zeroes of x and y have been relocated to the x-point. Distances are in ion inertial lengths, d_i. From Figs. 3c,d, the rates are roughly, $\gamma_x/\Omega_{e0} = 0.035$ and $\omega_y/\Omega_{e0} = 0.066$, where Ω_{e0} is the electron cyclotron frequency in B_0.

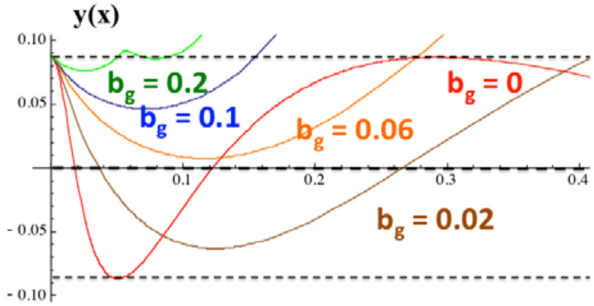

Figure 4 Parametric plots of y(x) sol'ns to Eqns (2) for $b_g = B_g/B_0 = 0, 0.02, 0.06, 0.1, 0.2$. M/m = 1836

The initial position of a characteristic[xi] trajectory is chosen as $x_0 = 0$ and $y_0 = 0.09d_i$ The initial y-drift velocity at y_0 is taken from the simulation to be $\dot{y}_0 = -0.2v_{eth}$. A small initial velocity, $\dot{x}_0 = 0.2v_{eth}$ is chosen, consistent with E_x.

At $\{x_0, y_0\}$ the downward moving electron begins to feel the y-force, which eventually turns it back up again in y as it is accelerated in x. When $B_g = 0$,$-x(t)$ □ $\sinh(\gamma_x t)$ and $y(t)$ □ $\cos(\omega_y t)$. For $B_g = 0.1B_0$, both x and y are linear combinations of $\sinh(\gamma' t)$, $\cosh(\gamma' t)$, $\sin(\omega' t)$ and $\cos(\omega' t)$, so that y is now growing as well as oscillating. Here, ω' and γ' are solutions to the eigenvalue equation for the linear eqns. (2):

$2\left\{\omega'^2,\ -\gamma'^2\right\} = \left[\Omega_{eg}^2 + \left(\omega_y^2 - \gamma_x^2\right)\right] \pm \sqrt{4\omega_y^2\gamma_x^2 + \left[\Omega_{eg}^2 + \left(\omega_y^2 - \gamma_x^2\right)\right]^2}$. In Fig. 4 the *parametric trajectories* y(x) are plotted for $B_g/B_0 = 0, 0.02, 0.06, 0.1$ and 0.2. For $B_g = 0$, the trajectory is bounded in y and extends out in x. For $B_g \neq 0$ the trajectories are all unbounded in y and leave the jet region at smaller and smaller x as B_g increases.

Reconnection simulations of jets in a guide field at later times

In order to study jets and diffusion regions at *later* times we have performed additional implicit PIC reconnection simulations with a mass ratio of M/m = 256 in a much larger simulation box of size $30d_i$ x $200d_i$. Time-histories of the reconnection rate (□ $-E_z(t)$) at the x-point are shown in Fig. 5a, together with v_{ex}/v_{eth0} at a late time.

For $B_g = 0$ (Fig. 5b) the jets are well collimated and undeflected for as long as the simulation is run ($t\Omega_i = 48$). Well-collimated jets are seen (Fig. 5b) emanating from the x-line to the left and from the x-lines of the island. For $B_g = 0.1B_0$ the jets are deflected throughout the simulation, including at the late time $t\Omega_i = 28$ (Fig. 5c) when the reconnection rate has plateaued.

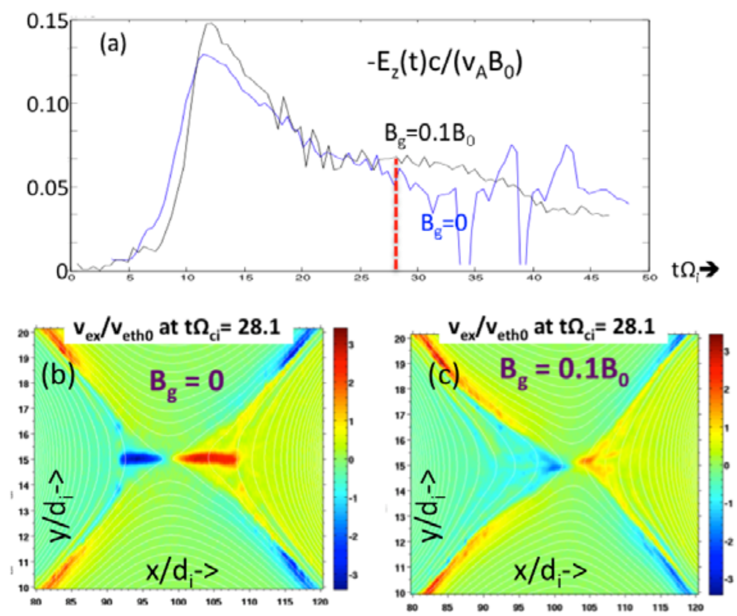

Figure 4: M/m = 256. (a): Reconnection rate, $-E_z(t)$, (inflow drift)/(inflow Alfven speed) near x-point for B_g=0, $0.1B_0$. (b,c): $v_{ex}(x,y)/v_{eth0}$ at time $t\Omega_i$= 28.1 for B_g = 0, $0.1B_0$

Using an even lower mass ratio M/m = 25, we find that the jets are only slightly deflected for guide fields as large as $B_g = 0.2B_0$. Therefore, the actual deflection of jets by small guide fields may be underestimated for unphysically small mass ratios.

Summary and significance

Just as has been found in standard models of 2D MHD,[iv] a number of features of magnetic reconnection found in "standard" antiparallel 2D *kinetic* simulations are not robust enough to survive even very small modifications to the initial conditions. New implicit 2D PIC simulations of reconnection have revealed that surprisingly small guide fields can distort and deflect the collimated electron jets in v_{ex} found in PIC simulations initiated with a "standard" antiparallel geometry, in which there is no guide field. For a physical mass ratio of M/m = 1836, a guide field, B_g, as small as one-twentieth of the asymptotic reversing field in the initial Harris equilibirum, B_0, is sufficient to deflect early-forming jets. A dynamical treatment of electron dynamics very close to the x-point during small guide field reconnection in a hydrogen plasma reveals the mechanism by which the Lorentz force of the guide field produces jet deflection for small guide fields. Early jet disruption by a guide field $B_g = 0.1B_0$ can sustained over long times, after the reconnection rate has begun to flatten, according to additional simulations with M/m = 256. The reconnection rate is essentially unchanged with the addition of such a small guide field, even though the narrow well-collimated "outer diffusion regions" of "standard" *antiparallel* reconnection simulations is destroyed along with the jets.

However, weak guide-field jet deflection found in these new simulations is at odds with the interpretation of recent measurements as undeflected electron jets along x in the presence of a weak guide field (Fig. 1). A resolution of this discrepancy may be possible through a reinterpretation of the observations. For example, the geometry of the reconnection exhaust depicted in Ref. vii, Fig. 2, could be generalized to allow for a deflected jet. Alternatively, this discrepancy *may* suggest shortcomings in modeling reconnection in the magnetosheath using widely accepted simulation approximations. Preliminary studies show that the colder electron temperatures in the sheath are probably not responsible for the discrepancy. Jet-deflection also appears to persist in 3D PIC simulations.

Whatever the resolution, almost all real reconnection events involve small guide fields and their effect on electron jets and on other features of reconnection need to be understood. Measurement of such electron features of magnetic reconnection will be one of the main thrusts of the upcoming NASA Magnetospheric Multiscale (MMS) mission and kinetic simulations must become more realistic in order to interpret such measurements physically.

Acknowledgement

This work was supported by NASA MMS Grant NNX08AO84G. We wish to thank Jan Egedal, Tai Phan, Forest Mozer and Michael Shay for useful discussions.

References

---

[i] M. A. Shay *et al.*, Phys. Rev. Lett. **99**, 155002 (2007)

[ii] H. Karimabadi, et al, Geophys. Res. Lett. **34** (2007)

[iii] K. Fujimoto, Phys. Plasmas **13**, 072904 (2006)

[iv] W. H. Matthaeus and S. L. Lamkin, Phys. Fluids **28**, 303 (1985); Phys. Fluids **29**, 2513 (1986); G. Lapenta, et al, Phys Rev Lett., 2007; P. Dmitruk and W.H. Matthaeus, Phys. Fluids 13, 042307, 2006; S. Servidio, et al, , Phys. Rev. Lett. **102**, 115003 (2009)

[v] Swisdak, *et al,* J. Geophys. Res., **110**, A05210 (2005) ; Karimabadi, *et al,* J. Geophys. Res., **110**, A03213 (2005)

[vi] G. Lapenta, *et al*, Phys. Plasmas **17**, 082106 (2010); S. Markidis, *et al*, Mathematics and Computers in Simulation, 1509, **80** (2010)

[vii] T. D. Phan, *et al,* Phys. Rev. Lett. **99**, 255002 (2007)

[viii] Hesse, et al. Phys. Plasmas **6**, 1781 (1999)

[ix] A. Le, *et al*, Physics of Plasmas **17**, 055703 (2010); Geophys. Res. Lett. **37**, L03106 (2010)

[x] T.W. Speiser, J. Geophys. Res., **70**, 4219 (1965)

[xi] Trajectories with many different initial conditions were studied both analytically and numerically, using forces from simulations. All were found to accelerate in x and oscillate in y as found for this characteristic trajectory.